Original Article

MOLECULAR METABOLISM

Mitochondrial uncoupling in the melanocortin system differentially regulates NPY and POMC neurons to promote weight-loss

Natalie Jane Michael [1], Stephanie Elise Simonds [1], Marco van den Top [3], Michael Alexander Cowley [1], David Spanswick [2,3,4,*]

ABSTRACT

Objective: The mitochondrial uncoupling agent 2,4-dinitrophenol (DNP), historically used as a treatment for obesity, is known to cross the blood-brain-barrier, but its effects on central neural circuits controlling body weight are largely unknown. As hypothalamic melanocortin neuropeptide Y/agouti-related protein (NPY/AgRP) and pro-opiomelanocortin (POMC) neurons represent key central regulators of food intake and energy expenditure we investigated the effects of DNP on these neurons, food intake and energy expenditure.

Method: C57BL/6 and melanocortin-4 receptor (MC4R) knock-out mice were administered DNP intracerebroventricularly (ICV) and the metabolic changes were characterized. The specific role of NPY and POMC neurons and the ionic mechanisms mediating the effects of uncoupling were examined with *in vitro* electrophysiology performed on NPY hrGFP or POMC eGFP mice.

Results: Here we show DNP-induced differential effects on melanocortin neurons including inhibiting orexigenic NPY and activating anorexigenic POMC neurons through independent ionic mechanisms coupled to mitochondrial function, consistent with an anorexigenic central effect. Central administration of DNP induced weight-loss, increased BAT thermogenesis and browning of white adipose tissue, and decreased food intake, effects that were absent in MC4R knock-out mice and blocked by the MC4R antagonist, AgRP.

Conclusion: These data show a novel central anti-obesity mechanism of action of DNP and highlight the potential for selective melanocortin mitochondrial uncoupling to target metabolic disorders.

Keywords Mitochondrial uncoupling; NPY; POMC; Weight-loss; BAT thermogenesis; ATP-sensitive potassium channel

1. INTRODUCTION

Mitochondrial uncoupling is a physiologically regulated process whereby a proton leak across the inner membrane is established, activity of the respiratory chain is dissociated from ATP synthesis, and energy is released as heat. Mammals, including humans, use uncoupling proteins in brown (BAT) and beige/brite adipose tissue to generate heat to support and maintain core body temperature. The recent realization that adult humans possess functional, active BAT [1–6], physiologically uncoupled through uncoupling protein-1 (UCP1), has reignited interest in BAT activation and thermogenesis as therapeutic targets for obesity and metabolic disorders [7–10].

Of the central neural effector pathways controlling food intake and energy balance, including BAT thermogenesis, the hypothalamus is critical [11–13]. The melanocortin system, with its origins in the arcuate nucleus (ARC), is comprised of orexigenic neuropeptide Y/agouti related protein (NPY/AgRP) and anorexigenic pro-opiomelanocortin (POMC) neurons. Both NPY/AgRP and POMC neurons are critical for the maintenance of food intake, energy balance, and glucose homeostasis [13], and activation of either neuronal phenotype influences BAT [14–17]. Both of these neuronal populations both express UCP2, a mitochondrial anion carrier that suppresses ATP production by compromising the mitochondrial inner membrane proton gradient and uncoupling oxidative phosphorylation [18,19]. Mitochondrial dynamics are regulated by nutrition in an opposing manner in NPY/AgRP and POMC neurons [20,21], and UCP2-mediated ROS production regulates functional activity of these neurons in opposing directions [19,22,23]. The role of UCP2 and mitochondrial dynamics in differentially regulating electrical excitability of NPY/AgRP and POMC neurons raises the interesting possibility of targeting mitochondrial uncoupling at the level of the melanocortin system as a potential strategy to influence energy balance and obesity.

[1]Metabolic Disease and Obesity Program, Biomedicine Discovery Institute, Monash University, Australia[5] [2]Neuroscience Program, Biomedicine Discovery Institute, Monash University, Australia[5] [3]Neurosolutions, Coventry, P.O. 3517, UK [4]Metabolic and Vascular Health, Warwick Medical School, University of Warwick, Coventry, CV4 7AL, UK

[5] Department of Physiology, 26 Innovation Walk, Monash University, Clayton, VIC 3800, Australia.

*Corresponding author. Neuroscience Program, Biomedicine Discovery Institute, Monash University, Australia.

E-mails: Natalie.michael@monash.edu (N.J. Michael), Stephanie.simonds@monash.edu (S.E. Simonds), Mvandentop@neurosolutionsltd.com (M. van den Top), Michael.cowley@monash.edu (M.A. Cowley), David.Spanswick@monash.edu (D. Spanswick).

Received April 26, 2017 • Revision received June 29, 2017 • Accepted July 5, 2017 • Available online 8 July 2017

http://dx.doi.org/10.1016/j.molmet.2017.07.002

To address this, we investigated the effects of central mitochondrial uncoupling on NPY/AgRP and POMC neuron activity and function. We utilized the prototypical mitochondrial uncoupler 2,4-dinitrophenol (DNP) to chemically induce uncoupling and investigate these effects on central melanocortin signaling. As NPY/AgRP and POMC neurons are known to couple their electrical excitability to energy status [24], and mitochondrial uncoupling disrupts the normal conversion of ADP and phosphate to ATP [25,26], we hypothesized that the electrical activity of these neurons would be differentially affected by mitochondrial uncoupling and drive changes in whole body energy homeostasis in favor of increased energy expenditure and weight loss. Thus, we tested the effects of centrally administered DNP *in vivo*.

2. METHODS

2.1. Mice

Mice were maintained on a 12 h light—dark cycle in a temperature-controlled, high barrier facility with free access to food and water. All experiments were approved by the Monash University School of Biomedical Sciences Animal Ethics Committee.

2.2. Metabolic measurements

Singly housed mice were acclimated for 24 h and monitored for 48 h in an environmentally controlled Comprehensive Lab Animal Monitoring System (CLAMS; Columbus Instruments, Columbus. OH). The system was fitted with indirect open circuit calorimetry and food consumption and activity monitors to measure activity, food intake, and energy expenditure. Energy expenditure and the respiratory exchange ratio (RER $= V_{CO_2}/V_{O_2}$) were calculated from gas exchange data.

2.3. Telemetric transponder implantation, locomotor activity, BAT, and core temperature measurements

Interscapular BAT temperature and locomotor activity were monitored by remote biotelemetry with pre-calibrated sensitive transmitters (PDT-4000 G2 E-Mitter sensors, Mini Mitter Company, Starr Life Science, Holliston, MA), as described previously [27]. E-Mitters were implanted beneath the BAT pad between the scapulae under isoflurane anesthesia and mice had 1 week for recovery before measurements commenced. Emitted transmitter signals were detected by a receiver positioned beneath the animal's home cage and analyzed using VitalView software (Mini Mitter Company, Starr Life Science, Holliston, MA). Locomotor activity counts are a relative measure of gross motor activity. For all experiments, activity counts and interscapular temperature measurements were obtained continually at 1 min intervals.

2.4. Sympathetic denervation

Methods for sympathetic denervation have been described previously [28]. Briefly, 8—12 week-old C57BL/6 male mice received 20 microinjections of 6-hydroxydopamine [6-OHDA (Sigma); 1 μL per injection, 9 mg/ml in 0.15 M NaCl containing 1% (w/v) ascorbic acid], or an equal volume of vehicle, throughout the right inguinal fat pads. Body weight was monitored throughout the duration of the experiment. Two weeks after 6-OHDA injections, mice were culled, and inguinal WAT and BAT were either formalin-fixed for histological/immunohistochemical assessment or processed for quantitative real time PCR.

2.5. Lateral ventricle cannulation and intracerebroventricular (ICV) drug administration

8—10 week old C57BL6/J mice were implanted stereotaxically with guide cannulas into the right lateral ventricle (0.2 mm posterior, 1 mm lateral from bregma) under 2% (v/v) isoflurane in 1 L/min oxygen. The tip of the guide cannula was positioned 1 mm above the injection site (1 mm ventral to the surface of the skull). Animals were allowed 4—5 days to recover. Following recovery, mice received artificial cerebrospinal fluid (aCSF; 1 μL) for 5 consecutive days and then were injected ICV with vehicle (aCSF) or AgRP and subsequently vehicle or DNP (1 μL—100 μM) for three consecutive days. For all *in vivo* experiments, 2, 4-dinitrophenol (DNP, Sigma) was made up as a concentrated stock in DMSO, which was then diluted into aCSF. All vehicle treated mice, were treated with aCSF with the addition of DMSO. Physiological measurements outlined were recorded throughout this period.

2.6. Real-time PCR

Real-Time PCR procedures were fundamentally the same as those described previously [29]. Briefly, RNA was extracted using TRIzol reagent (Invitrogen, Carlsbad, CA), and total RNA quality and quantity was determined using a NanoDrop 3300 (Thermo Scientific, Wilmington, DE, USA). mRNA was reverse transcribed using a High-Capacity cDNA Reverse Transcription Kit (Applied Biosystems, Foster City, CA) and processed for quantitative real-time PCR using SsoAdvanced Universal SYBR Green Supermix (Bio-Rad, Hercules, CA). Inguinal white adipose gene comparisons used TATA boxbinding protein (Tbp) as the housekeeping gene, all other expression studies were normalized to Gapdh. The following primers were used: *Ucp-1* (f-ACTGCCACACCTCCAGTCATT, r-CTTTGCCTCACTCAGG ATTGG), *Tbp* (f-GAAGCTGCGGTACAATTCCAG, r-CCCCTTGTACCCTTC ACCAAT), *Gapdh* (f-ACCACAGTCCATGCCATCAC, r-CACCACCCTGTTGCTGTA GCC).

2.7. Histology and WAT immunohistochemistry

Hematoxylin and eosin staining and UCP1 DAB staining were performed on intact and de-innervated inguinal WAT fat pads from DNP and vehicle treated animals as described previously [see 28]. Briefly, animals were killed and inguinal fat immediately dissected and fixed in buffered formalin solution for 48 h. Tissues were embedded in paraffin and 4 μm sections of the entire block prepared. Every tenth to fourteenth section of the tissue was used to detect UCP-1 staining as previously described [29].Sections were incubated overnight (4 °C) with anti-UCP-1 (1:1000; ab10983, Abcam, San Francisco, CA). After washing sections were incubated for 2 h at room temperature with Alexa-Fluor 488-conjugated secondary antibodies (1:1000; Life Technologies, VIC, Australia).

2.8. Electrophysiology

Male, 6—10 week old, NPY renilla GFP and POMC eGFP-expressing transgenic mice were used for electrophysiological studies, as previously described [30,31]. Animals were terminally anaesthetized with isoflurane, decapitated, and the brain rapidly removed; 250 μm coronal hypothalamic brain slices were cut in a modified, sucrose-based, ice-cold artificial cerebrospinal fluid (aCSF) using a Leica VT1000S vibratome. Slices were rapidly warmed to 34° for 20 min before being returned to room temperature prior to recording. The composition of artificial cerebrospinal fluid (aCSF) was (in mM): 127 NaCl; 1.9 KCl; 1.2 KH_2PO_4; 2.4 $CaCl_2$; 1.3 $MgCl_2$; 26 $NaHCO_3$; 2 D-glucose; 8 Manitol, equilibrated with 95% O_2—5% CO_2, except when slices were being cut when NaCl was replaced with equimolar sucrose (127 mM). Whole-cell recordings were performed under visual control using fluorescence and differential interference contrast optics with infrared video microscopy (Axioskop FS2; Zeiss). POMC and NPY neurons were visually identified in the ARC by their expression of GFP and whole-cell patch-clamp recordings obtained using an Axopatch 1D amplifier (MDS Analytical Technologies). Patch-pipettes were manufactured from thin-walled borosilicate glass (Harvard Apparatus; GC150-TF10) using a

horizontal electrode puller (Sutter Instruments, USA; Model P1000) and had resistance 5–10 MΩ when filled with intracellular recording solution of the following composition: 140 potassium gluconate; 10 KCl; 1 EGTA-Na; 10 HEPES; 2 Na_2ATP; osmolarity, and pH adjusted with sucrose and KOH, respectively. Signals were displayed on a digital oscilloscope (Tektronix TDS1002) and stored on a desk top computer with currents filtered at 2 kHz. In current clamp recordings, baseline activity, resting membrane potential and active conductance profile were assessed before any experimental manipulations. In voltage clamp experiments, cells were held at −60 mV, and currents were elicited with a voltage ramp from −120 to −30 mV at a rate of 8 mV/s. All signals were captured on a personal computer running pClamp 9.2 (MDS Analytical Technologies). Any cell that did not display a stable baseline membrane potential, was running up, or displayed deterioration in action potentials was excluded from data analysis. These criteria were established before data collection.

The following drugs were used for electrophysiological experiments: 2,4-dinitrophenol (DNP, Sigma); and tolbutamide (Sigma) were made up as concentrated stocks in DMSO and ethanol respectively and stored at <−4 °C; SN-6 (Tocris), oubain octahydrate (Sigma), $BaCl_2$ (Sigma), and TTX (Abcam) were made up as concentrated stocks in distilled water and stored at <−4 °C, apart from $BaCl_2$ which was stored <4 °C. Drugs were diluted to the required concentration in aCSF immediately prior to use. All drugs were applied to the slice by perfusion from gravity-fed reservoirs connected to the main perfusion line via 3-way valves.

2.9. Data analysis

All *ex vivo* analysis was conducted using Clampfit (MDS Analytical Technologies). All data are presented as means ± SEM. Two-tailed paired *t*-tests were generated using GraphPad Prism 6 for comparisons between conditions. Parametric statistics were used when the data from both conditions adopted a Gaussian distribution, and non-parametric statistics were used when this assumption was not met. For molecular and *in vivo* experiments, statistical significance was determined by either a two-way ANOVA or a two-tailed paired Student's *t*-test. *p* values < 0.05 were considered significant; $^*p < 0.05$, $^{**}p < 0.01$, $^{***}p < 0.001$, and were adjusted when multiple comparisons were performed.

3. RESULTS AND DISCUSSION

3.1. ICV DNP promoted weight loss via increased BAT thermogenesis and WAT browning

Intracerebroventricular (ICV) DNP (1 μL of 100 μM) induced significant weight-loss ($p < 0.01$ DNP compared to vehicle control; day 2 and 3 of treatment, day 1 of recovery; Figure 1A), increased energy expenditure via increased BAT thermogenesis ($p < 0.01$ versus vehicle control, day 1 of treatment; Figure 1B), and significantly decreased food intake at day 3 of treatment ($p < 0.01$ versus vehicle control; Figure 1C). Intraperitoneal (IP) administration of DNP had similar effects on body weight and food intake (Figure S1A and B). Browning was visibly evident in the interscapular BAT depot (Figure S1C), and uncoupling protein 1 (UCP1) mRNA in both BAT and inguinal white adipose tissue (ingWAT) were significantly elevated following ICV treatment with DNP ($p < 0.05$ and $p < 0.001$ for BAT and WAT, respectively compared to vehicle, Figure 1D); the latter was consistent with increased "browning" of WAT. Denervated WAT did not result in increased UCP-1 expression following central DNP administration ($p > 0.05$; Figure 1D) or IP administration (Figure S1E). Innervated inguinal WAT in DNP-treated animals also displayed morphology more consistent with that of brown fat [32]: small adipocyte clusters with multilocular lipid droplets (Figure S1D). These effects of DNP were absent in the ipsilateral sides of sympathetically denervated mice, indicating effects of DNP were neural in origin and centrally driven (Figure 1D and E). Core body temperature was found to be significantly increased in DNP treated animals with no obvious indications of changes in physical activity (data not shown). Acute DNP treatment did not result in any significant changes in RER, and only a mild change in V_{O_2} consumption was recorded (Figure S1F).

3.2. ICV effects of DNP were mediated via the melanocortin system

To confirm these effects of central DNP were mediated via the melanocortin system, we tested the effects of the endogenous MC4R antagonist AgRP on DNP-induced changes in body weight, food intake, and BAT thermogenesis. ICV DNP (100 μM) in the presence of AgRP (1 nmol, ICV) had no appreciable effect on body weight or BAT thermogenesis (Figure 1F and G). AgRP alone significantly increased food intake on day 1 of treatment, but DNP failed to induce any effect on food intake at any time point ($p < 0.05$ for AgRP treated versus DNP + AgRP treated, day 1 treatment; Figure 1H). We next tested the effects of DNP in MC4R knock-out mice. DNP was without significant effect on body weight, BAT thermogenesis, and food intake (Figure 1I–K). Collectively, these data indicate that central DNP-induced effects on energy expenditure, food intake, and body weight are mediated via the melanocortin system.

3.3. DNP inhibits ARC NPY neurons via opening of KATP

To determine underlying mechanisms by which chemical uncoupling of the melancortin system induced weight-loss and increased energy expenditure, we investigated effects of chemically-induced mitochondrial uncoupling on electrical excitability of NPY and POMC neurons. Whole-cell patch clamp recordings were obtained from NPY and POMC neurons in adult mouse hypothalamic brain slices prepared from transgenic mouse strains in which NPY or POMC expressed green fluorescent protein (GFP; [30,31]). Briefly, bolus bath application of 200 μM DNP induced inhibition of NPY neurons (15/17). This effect was characterized by membrane hyperpolarization of 11.6 ± 2.3 mV, from a mean resting potential of −42.0 ± 2.2 mV to a peak steady-state of −53.6 ± 2.7 mV in DNP ($n = 14$, paired *t*-test, $t_{(13)} = 5.04$, $p < 0.001$), and significant reduction in spontaneous firing rate in active cells ($n = 7$, Wilcoxon matched-pairs signed-rank test, $W = -28$, $p < 0.05$) (Figure 2A and B). DNP-induced inhibition was associated with a 47.0 ± 5.8% decrease in input resistance, from 1638 ± 270 MΩ to 721 ± 137 MΩ ($n = 14$, Wilcoxon matched-pairs signed-rank test, $W = -105$, $p < 0.01$) and persisted in tetrodotoxin (TTX) (500 nM) ($n = 4$ cells), indicating a direct effect of DNP on NPY neurons (Figure 2C–E). Reversal potentials of DNP-induced membrane conductance amounted to −69.5 ± 3.9 mV ($n = 12$), and −65.2 ± 6.8 mV ($n = 3$) in the presence of TTX. Voltage-clamp experiments (Vhold −60 mV), in TTX, demonstrated outward currents underlie DNP-induced inhibition ($n = 6$) (Figure 2C–E).

DNP-induced inhibition persisted in chloride-loaded cells ($n = 11$) (data not shown) but was reversed by the ATP-sensitive potassium channel (K_{ATP}) blocker tolbutamide (200 μM; $n = 8$) (Figure 2B–E). Following DNP-induced membrane hyperpolarisation, subsequent application of tolbutamide induced membrane depolarisation of 15.8 ± 2.0 mV ($n = 8$, paired *t*-test, $t_{(7)} = 8.02$, $p < 0.001$) associated with a 320 ± 126% increase in input resistance ($n = 4$, $p < 0.05$), from 432 ± 133 MΩ in DNP to 914 ± 131 MΩ in the presence of DNP and tolbutamide. Tolbutamide also restored spontaneous action potential firing to control, pre-DNP, levels (baseline 0.23 ± 0.14 Hz,

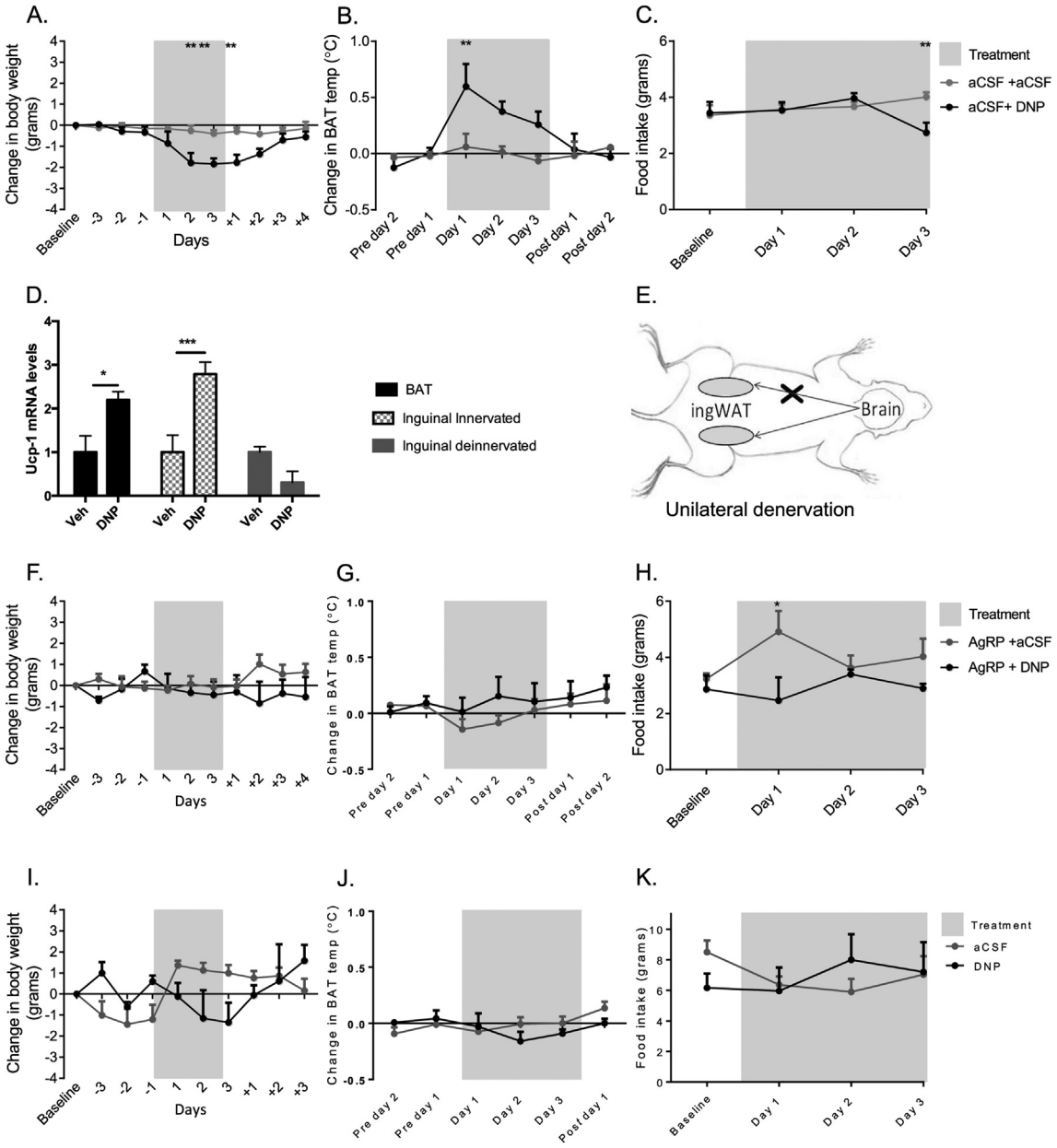

Figure 1: Uncoupling of the melanocortin system with centrally administered DNP induced weight-loss, increased BAT thermogenesis and WAT browning. The weight loss induced by DNP was eliminated by pre-treatment with AgRP, and was absent in MC4KO mice. (A–C) Effects of ICV DNP administration on body weight, BAT temperature, and food intake compared to aCSF vehicle ($n = 4$–5 per group). (D) UCP1 mRNA expression in BAT and ingWAT depots after ICV DNP or vehicle injections. (E) ingWAT was unilaterally denervated prior to ICV DNP or vehicle injections. (F–H) Effects of ICV administration of DNP on body weight, BAT temperature and food intake, after pre-treatment with AgRP ($n = 3$–6 per group). (I–K) Effects of ICV administration of DNP on body weight, BAT temperature and food intake in MC4KO mice ($n = 3$ for all conditions). All data Mean ± SEM. *$p < 0.05$, **$p < 0.01$.

tolbutamide 0.23 ± 0.17 Hz, $n = 4$). Taken together, these data indicate chemical uncoupling and inhibition of NPY neurons by DNP is mediated via opening of K_{ATP} channels.

3.4. DNP excites the majority of ARC POMC neurons via multiple mechanisms including block of Kir channels

In contrast to NPY neurons, mitochondrial uncoupling with DNP (200 μM) induced excitation in the majority of POMC neurons (59.3%, $n = 16$). The remaining POMC neurons were inhibited by DNP (33.3%, $n = 9$) in a manner similar to NPY neurons, via activation of K_{ATP} channels (see Figure S2A–F) or DNP induced a biphasic response: excitation followed by inhibition (7.4%, $n = 2$; data not shown).

DNP induced excitation of POMC neurons was characterized by membrane potential depolarization of 9.0 ± 1.4 mV ($n = 16$, paired t-test, $t_{(15)} = 6.51$, $p < 0.0001$) and significant increase in action potential firing rate from 0.91 ± 0.38 Hz to 3.75 ± 0.92 Hz in DNP ($n = 16$, Wilcoxon matched-pairs signed-rank test, W = 120, $p < 0.0001$; Figure 3A). DNP-induced excitation persisted in TTX

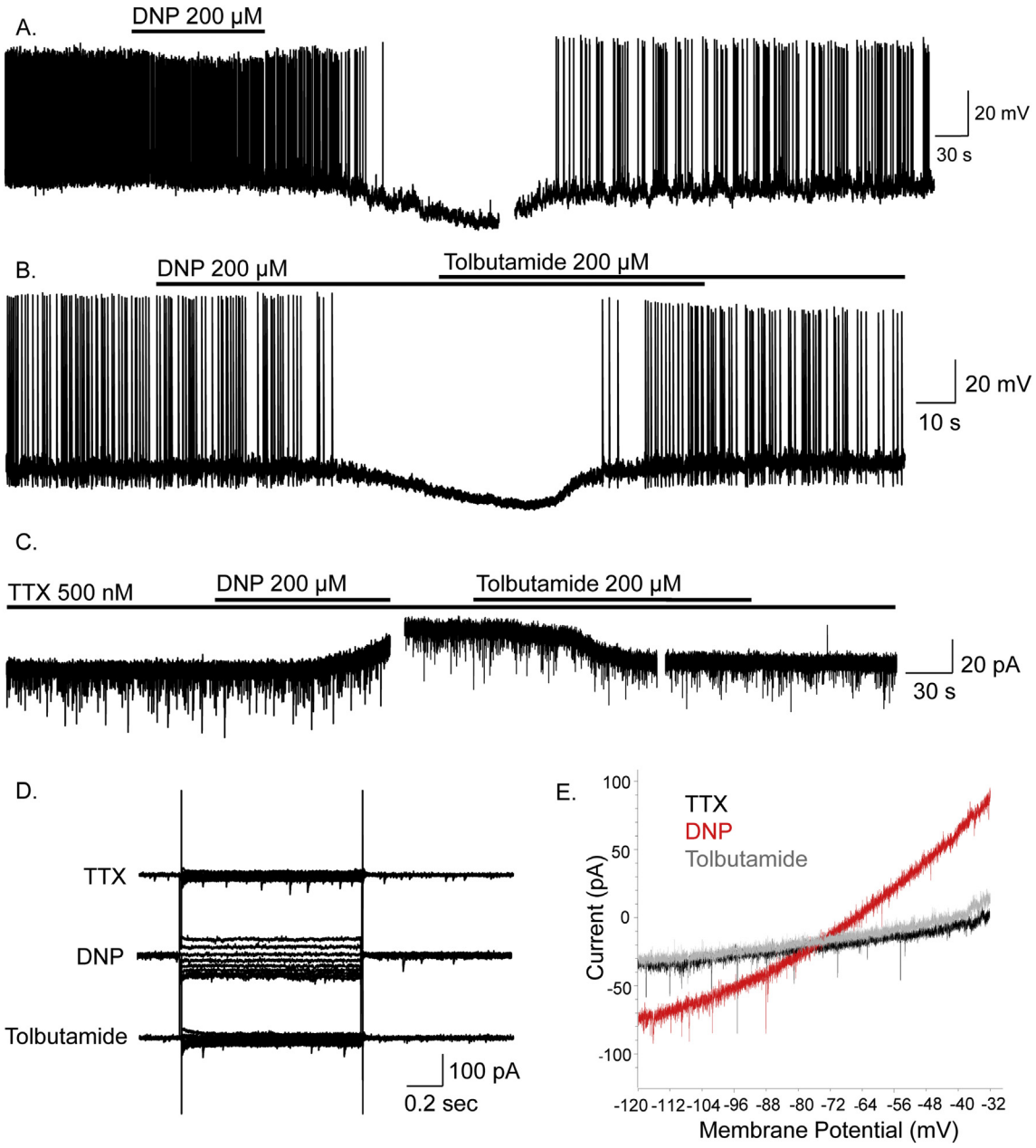

Figure 2: DNP inhibits ARC NPY neurons via activation of K_{ATP} channels. (A) Whole-cell recordings showing DNP induced hyperpolarisation and inhibition of an NPY neuron. (B) DNP-induced inhibition was reversed by tolbutamide. (C) DNP-induced inhibition and associated outward current was reversed by tolbutamide and persisted in TTX indicating a direct post-synaptic effect via activation of K_{ATP} channels. (D) Voltage-clamp recordings in TTX showing current-voltage relations in control, DNP and tolbutamide. (E) Current responses to voltage-clamp ramps (8 mV/s from −120 to −30 mV; Vhold −60 mV) for control (black), DNP (red) and tolbutamide (grey), all in the presence of TTX. These data indicate DNP induced inhibition of NPY neurons is via activation of K_{ATP}.

(500 nM) ($n = 7$) indicating a direct effect of DNP on POMC neurons (Figure 3B) and was associated with an inward current, observed in voltage-clamp at a holding potential of −60 mV (data not shown). Current-voltage relations (IV's) in the presence and absence of DNP revealed DNP-induced excitation associated with an increase, decrease, or no measurable change in neuronal input resistance, suggesting DNP-induced excitation was associated with multiple ionic mechanisms. In 15 POMC cells that expressed instantaneous inwardly rectifying potassium conductances (K_{IR}) DNP-induced excitation was associated with a reduction in inward rectification (Figure 3C and D). To confirm DNP-induced excitation was via block of inward rectification, we tested the effects of the K_{IR} blocker Ba^{2+} (100 μM) on DNP-induced depolarization in POMC neurons expressing this conductance. Ba^{2+} mimicked the effects of DNP inducing membrane depolarisation of 10.3 ± 2.0 mV associated with an increase in neuronal input resistance (Figure 3E) and block of K_{IR} ($n = 13$, paired t-test, $t_{(12)} = 5.22$, $p < 0.001$; Figure 3F and G). DNP-induced excitation was completely blocked by Ba^{2+} in 6/13 POMC neurons. Thus DNP-induced excitation was mediated in part via block of K_{IR}, although other mechanisms clearly contribute. IV relations revealed the remaining DNP-induced excitations were associated with a parallel shift, the lack of change in whole-cell

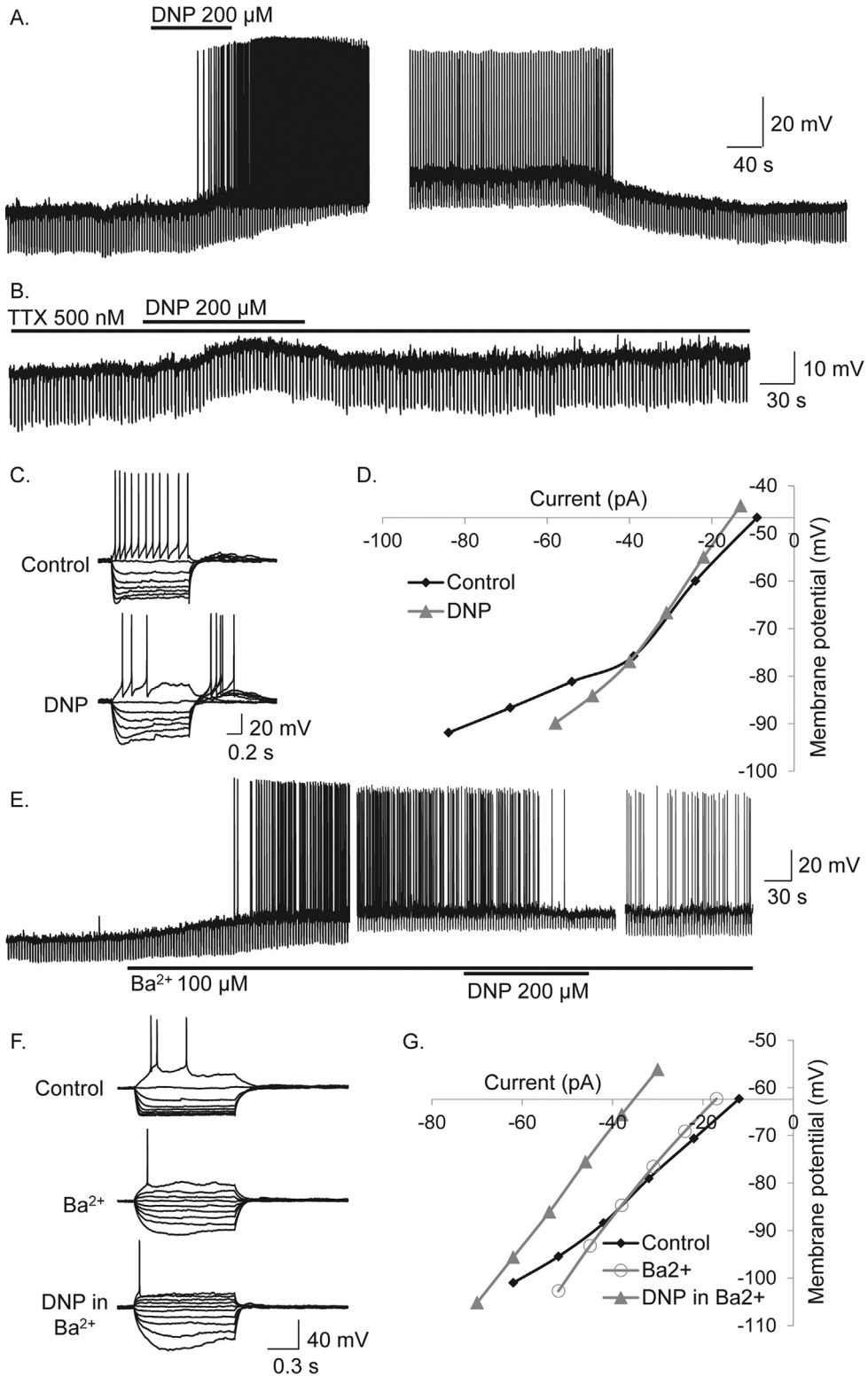

Figure 3: DNP activates anorexigenic POMC neurons via block of an inwardly rectifying potassium conductance. (A) DNP-induced a reversible excitation and action potential firing in a POMC neuron. (B) DNP-induced excitation, persisted in TTX, indicating a direct postsynaptic site of action. (C) Voltage-current relations in control and in the presence of DNP revealed DNP induced an increase in neuronal input resistance and inhibition of inward rectification, seen at more negative membrane potentials and indicated by the reduction in the non-linear voltage responses to large amplitude current injection observed in control. (D) Plot of data shown in C. Note the non-liner current voltage-relations in control and subsequent reduction in DNP indicating DNP-induced excitation via block of an inwardly rectifying potassium conductance (K_{IR}). (E) The K_{IR} blocker Ba^{2+} mimicked and occluded DNP-induced excitation. (F) Voltage-current (VI) relations show inward rectification observed was blocked by Ba^{2+}, DNP having no further effect on this conductance. (G) Plot of VI relations showing Ba^{2+}-induced block of inward rectification and DNP-induced subsequent effects associated with a parallel shift and no obvious change in conductance, suggesting modulation of ion pumps/exchangers.

conductance suggesting ion pumps/exchangers may contribute to DNP-induced excitation. Hence, we investigated effects of the sodium potassium ATPase pump (Na^+/K^+-ATPase) inhibitor Ouabain (100 μM). Ouabain mimicked effects of DNP and reduced DNP-induced excitation in 5/15 cells (Figure 4A and B). In a further 12 cells, DNP-induced excitation persisted in the presence of Ouabain (Figure 4C). We next tested the effects of the sodium calcium exchanger (NCX) SN-6 (20 μM). SN-6 completely blocked DNP-induced excitation in 4 POMC neurons (Figure 4D). Thus, DNP-induced mitochondrial uncoupling and excitation of POMC neurons is mediated via block of K_{IR}, the Na^+/K^+-ATPase and NCX.

Taken together, these data show that mitochondrial uncoupling inhibits orexigenic NPY and activates anorexigenic POMC neurons, promoting increased energy expenditure through activation of BAT thermogenesis, WAT browning, decreased food intake, and increased weight loss. This differential effect on these neurons is the ideal scenario to promote weight loss and highlights the potential of targeted mitochondrial uncoupling to treat obesity.

Uncoupling of NPY neurons induced inhibition via activation of K_{ATP} channels. Mechanistically, this is likely mediated via reducing endogenous ATP levels and reducing ATP-mediated inhibition of these channels, DNP acting as a protonophore to disrupt ADP conversion to ATP [25,26]. While a subpopulation of POMC neurons were inhibited by DNP in a manner analogous to that observed in NPY neurons, the vast majority were excited by DNP. In these cells, uncoupling induced excitation via block of the Na^+/K^+-ATPase, NCX, and K_{IR}. Tonic activity of these pumps/ion exchangers and K_{IR}, therefore, couple energy status to electrical excitability in POMC neurons. The effects of DNP persisted in the presence of TTX, suggesting a direct effect on the post-synaptic neuron rather than an indirect effect through activity-dependent, synaptic neurotransmitter release. However, we cannot eliminate an effect of DNP on presynaptic terminals innervating NPY and POMC neurons, neither can we eliminate an indirect effect of DNP via non-neuronal local networks of glia including astrocytes and tanycytes. In the latter case, chemical uncoupling of glia could lead to a reduction in ATP synthesis in these cells and loss of glia-neuronal signaling through ATP release via connexin hemi-channels, effectively removing an ATP and glia-dependent tonic drive to neurons [33]. Both glia-derived ATP and/or adenosine could form such a tonic drive, although in the case of NPY, glia-derived adenosine has been shown to inhibit these neurons [34]; thus, it is unlikely to underlie the effects observed here. Alternatively, chemical uncoupling of glia could disrupt release of lactate from these cells, lactate release from specific subtypes of tanycytes being suggested to regulate activity of both orexigenic NPY and anorexigenic POMC neurons [35,36]. At present, we do not know to what extent chemical uncoupling of glia contributes to the effects of DNP on neuronal excitability. Nevertheless, chemical uncoupling with DNP induces opposing effects on electrical activity of NPY and POMC neurons to reduce food intake, promote energy expenditure, and weight loss.

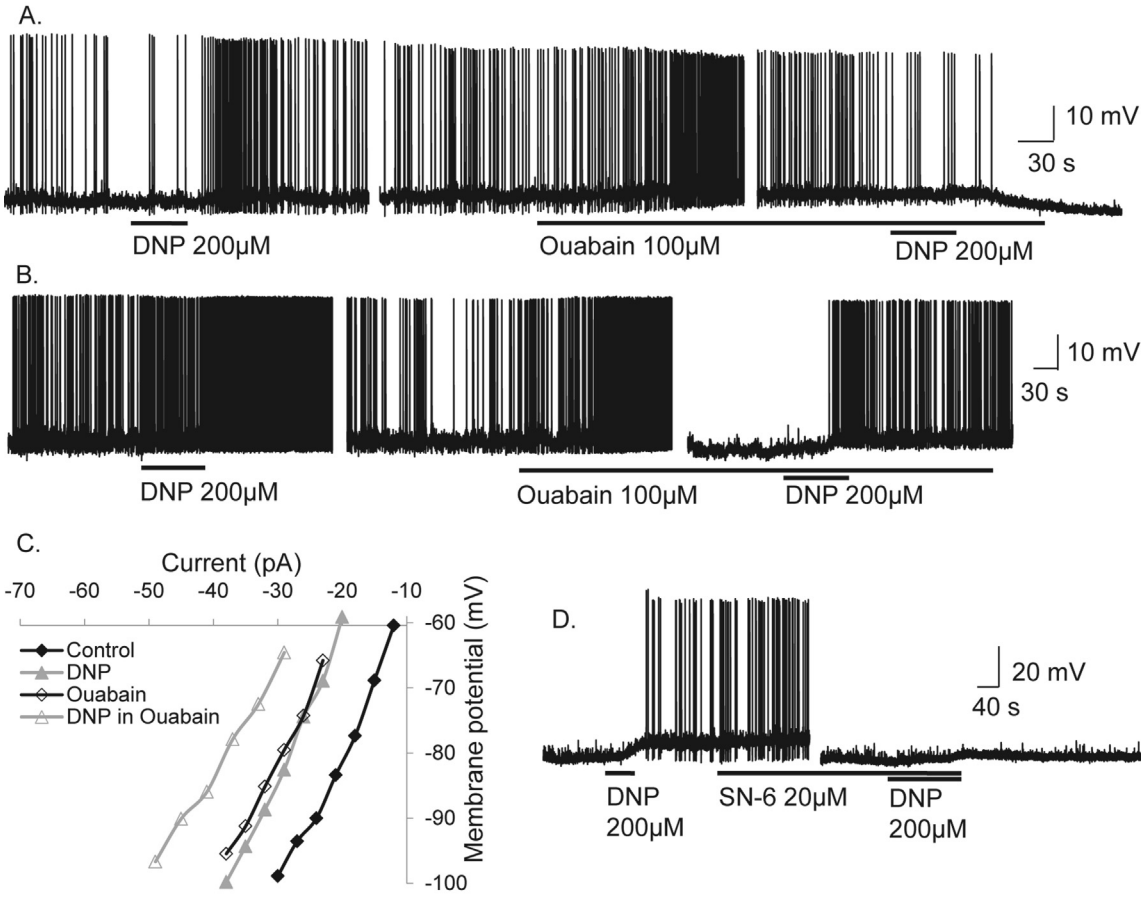

Figure 4: DNP also activates anorexigenic POMC neurons via the sodium potassium ATPase and sodium calcium exchange. (A) Whole-cell current clamp recordings from an ARC POMC neuron showing that DNP-induced excitation was blocked by the Na^+/K^+-ATPase inhibitor ouabain. (B) Recording from another POMC neuron showing DNP-induced excitation persisted in Ouabain. (C) Current-voltage relations reveal ouabain-sensitive and insensitive components contribute to DNP-induced excitation (D) Whole-cell recording from an ARC POMC neuron showing DNP-induced excitation was blocked by the NCX inhibitor SN-6.

That mitochondrial uncoupling induces opposing effects on orexigenic NPY and anorexigenic POMC neurons indicates that these neurons directly couple electrical excitability and activity to energy status and changes in the bioenergetics of these cells is translated into opposing electrophysiological outputs. Chemical uncoupling has distinct parallels with physiological uncoupling in the melanocortin system. In NPY/AgRP neurons, both fasting and the "hunger" hormone ghrelin maintain increased neuronal activity via a UCP2-dependent regulation of ROS levels, ablation of UCP2 reducing NPY/AgRP neuronal activity, ghrelin, and fasting-induced food intake [22,37]. Mitochondrial dynamics in NPY/AgRP neurons are also subject to plasticity; fasting promotes mitochondrial fission and high-fat diet-induced states of positive energy balance promoting mitochondrial fusion [20], and fasting also induces a UCP2-dependent increase in mitochondrial number in the arcuate nucleus [22]. Mitochondrial fission and glucose-induced neuronal activity are UCP2-dependent in ventromedial nucleus hypothalamic neurons [38]. Remarkably, mitochondrial dynamics in anorexigenic POMC neurons are regulated by nutrition in the opposite manner to NPY neurons [20,21], and K_{ATP}-dependent glucose-sensing in POMC neurons and lateral hypothalamic MCH neurons is regulated by UCP2 [23,39].

DNP has been known to induce rapid weight loss for decades, but its narrow therapeutic index and adverse side-effects have limited its utility. Overdose or over-exposure with DNP, a phenol-based structure, is characterized by classic symptoms that include hyperthermia, tachycardia, tachypnoea, and diaphoresis associated with cardiovascular failure and often death. Several mechanisms are suggested to contribute to DNP-induced toxicity [see 26]. Uncoupling of oxidative phosphorylation by DNP leads to a proton leak across the inner membrane being established, activity of the respiratory chain dissociated from ATP synthesis, and energy is released as heat. This loss of homeostatic control of thermoregulation effectively gives rise to uncontrolled hyperthermia [40]. Stimulation of glycolysis and increased pyruvic acid and lactic acid production along with potassium and phosphate accumulation have also been proposed to contribute to DNP-induced toxicity [see 26]. In experiments described here, changes in electrophysiological and *in vivo* whole animal physiological parameters recovered after cessation of exposure to DNP, suggesting results described here do not reflect pathophysiological effects of DNP. The adverse effects of DNP have been broadly highlighted, a factor that has contributed to the loss of interest in the therapeutic potential of such agents. However, the concept of mitochondrial uncouplers as therapeutics has recently regained momentum with the realization of a range of beneficial effects of mild mitochondrial uncoupling. DNP at low concentrations has been shown to improve neuronal function or to be neuroprotective in a range of animal models of disease including: epilepsy, experimental optic neuritis, Parkinson's disease, Alzheimer's disease, stroke, traumatic brain injury, and peripheral nerve injury [41–48]. Future therapeutic approaches targeting obesity with mitochondrial uncoupling agents will need a chronic dosing strategy that offsets any toxicity. Studies in mice housed at thermoneutrality with DNP administered via drinking water showed DNP to protect against diet-induced obesity: treated animals showing increased energy expenditure, decreased body weight and fat mass, compared to controls, with improved glucose tolerance and no obvious toxicity after around 2 months of exposure to DNP [49]. Mild mitochondrial uncoupling in neurons has been shown to reprogram mTOR and insulin signaling, up-regulate signaling pathways associated with adaptive stress responses and synaptic plasticity, and improve learning and memory [50]. Thus, new therapeutic approaches and strategies utilizing mitochondrial uncoupling agents to target obesity are worthy of further investigation.

4. CONCLUSION

In summary, using the original weight-loss inducing drug DNP, we have demonstrated here for the first time that chemical uncoupling of the melanocortin system promotes increased energy expenditure and weight loss through differentially regulating excitability of orexigenic NPY and anorexigenic POMC neurons. DNP is known to cross the blood-brain-barrier, and data presented here strongly support a key and novel mechanism by which chemical uncoupling agents targeting the melanocortin system, such as DNP, may offer new insight for future approaches to tackle obesity.

4.1. Data availability

The data supporting the findings of this study are presented within the manuscript and are available from the corresponding author upon request.

AUTHOR CONTRIBUTIONS

In vitro electrophysiology experiments performed, designed and analyzed by N.J.M., M.vdT., and D.S. *In vivo* physiology experiments were performed, designed and analyzed by S.E.S., M.A.C., and D.S. Manuscript was written by N.J.M., S.E.S, M.vdT, M.A.C, and D.S.

ACKNOWLEDGEMENTS

This work was supported by the National Health and Medical Research Council (NHMRC) of Australia (APP1063955 and APP1084600 to D.S. and APP1079422 and APP1065641 to M.A.C.). This funding source had no role in the study design, data collection, analysis, or interpretation, the writing of the report, or in the decision to submit the article for publication.

CONFLICT OF INTEREST

The authors declare no conflicts of interest.

APPENDIX A. SUPPLEMENTARY DATA

Supplementary data related to this article can be found at http://dx.doi.org/10.1016/j.molmet.2017.07.002.

REFERENCES

[1] Chondronikola, M., Volpi, E., Borsheim, E., Porter, C., Saraf, M.K., Annamalai, P., et al., 2016. Brown adipose tissue activation is linked to distinct systemic effects on lipid metabolism in humans. Cell Metabolism 23(6):1200–1206.

[2] Cypess, A.M., Lehman, S., Williams, G., Tal, I., Rodman, D., Goldfine, A.B., et al., 2009. Identification and importance of brown adipose tissue in adult humans. The New England Journal of Medicine 360(15):1509–1517.

[3] Lidell, M.E., Betz, M.J., Dahlqvist Leinhard, O., Heglind, M., Elander, L., Slawik, M., et al., 2013. Evidence for two types of brown adipose tissue in humans. Nature Medicine 19(5):631–634.

[4] Ouellet, V., Labbe, S.M., Blondin, D.P., Phoenix, S., Guerin, B., Haman, F., et al., 2012. Brown adipose tissue oxidative metabolism contributes to energy expenditure during acute cold exposure in humans. Journal of Clinical Investigation 122(2):545–552.

[5] van Marken Lichtenbelt, W.D., Vanhommerig, J.W., Smulders, N.M., Drossaerts, J.M., Kemerink, G.J., Bouvy, N.D., et al., 2009. Cold-activated

brown adipose tissue in healthy men. The New England Journal of Medicine 360(15):1500–1508.
[6] Virtanen, K.A., Lidell, M.E., Orava, J., Heglind, M., Westergren, R., Niemi, T., et al., 2009. Functional brown adipose tissue in healthy adults. The New England Journal of Medicine 360(15):1518–1525.
[7] Chechi, K., Nedergaard, J., Richard, D., 2014. Brown adipose tissue as an anti-obesity tissue in humans. Obesity Reviews 15(2):92–106.
[8] Tseng, Y.H., Cypess, A.M., Kahn, C.R., 2010. Cellular bioenergetics as a target for obesity therapy. Nature Reviews Drug Discovery 9(6):465–482.
[9] Nedergaard, J., Cannon, B., 2010. The changed metabolic world with human brown adipose tissue: therapeutic visions. Cell Metabolism 11(4):268–272.
[10] Whittle, A.J., Lopez, M., Vidal-Puig, A., 2011. Using brown adipose tissue to treat obesity – the central issue. Trends in Molecular Medicine 17(8):405–411.
[11] Labbe, S.M., Caron, A., Lanfray, D., Monge-Rofarello, B., Bartness, T.J., Richard, D., 2015. Hypothalamic control of brown adipose tissue thermogenesis. Frontiers in Systems Neuroscience 9:150.
[12] Contreras, C., Gonzalez, F., Ferno, J., Dieguez, C., Rahmouni, K., Nogueiras, R., et al., 2015. The brain and brown fat. Annals of Medicine 47(2):150–168.
[13] Cone, R.D., 2005. Anatomy and regulation of the central melanocortin system. Nature Neuroscience 8(5):571–578.
[14] Shi, Y.C., Lau, J., Lin, Z., Zhang, H., Zhai, L., Sperk, G., et al., 2013. Arcuate NPY controls sympathetic output and BAT function via a relay of tyrosine hydroxylase neurons in the PVN. Cell Metabolism 17(2):236–248.
[15] Kooijman, S., Boon, M.R., Parlevliet, E.T., Geerling, J.J., van de Pol, V., Romijn, J.A., et al., 2014. Inhibition of the central melanocortin system decreases brown adipose tissue activity. The Journal of Lipid Research 55(10):2022–2032.
[16] Zhang, Y., Kilroy, G.E., Henagan, T.M., Prpic-Uhing, V., Richards, W.G., Bannon, A.W., et al., 2005. Targeted deletion of melanocortin receptor subtypes 3 and 4, but not CART, alters nutrient partitioning and compromises behavioral and metabolic responses to leptin. The FASEB Journal 19(11):1482–1491.
[17] Burke, L.K., Doslikova, B., D'Agostino, G., Greenwald-Yarnell, M., Georgescu, T., Chianese, R., et al., 2016. Sex difference in physical activity, energy expenditure and obesity driven by a subpopulation of hypothalamic POMC neurons. Molecular Genetics and Metabolism 5(3):245–252.
[18] Nasrallah, C.M., Horvath, T.L., 2014. Mitochondrial dynamics in the central regulation of metabolism. Nature Reviews Endocrinology 10(11):650–658.
[19] Toda, C., Diano, S., 2014. Mitochondrial UCP2 in the central regulation of metabolism. Best Practice & Research Clinical Endocrinology & Metabolism 28(5):757–764.
[20] Dietrich, M.O., Liu, Z.W., Horvath, T.L., 2013. Mitochondrial dynamics controlled by mitofusins regulate Agrp neuronal activity and diet-induced obesity. Cell 155(1):188–199.
[21] Schneeberger, M., Dietrich, M.O., Sebastian, D., Imbernon, M., Castano, C., Garcia, A., et al., 2013. Mitofusin 2 in POMC neurons connects ER stress with leptin resistance and energy imbalance. Cell 155(1):172–187.
[22] Andrews, Z.B., Liu, Z.W., Walllingford, N., Erion, D.M., Borok, E., Friedman, J.M., et al., 2008. UCP2 mediates ghrelin's action on NPY/AgRP neurons by lowering free radicals. Nature 454(7206):846–851.
[23] Parton, L.E., Ping Ye, C., Coppari, R., Enriori, P.J., Choi, B., Zhang, C., et al., 2007. Glucose sensing by POMC neurons regulates glucose homeostasis and is impaired in obesity. Nature 449(7159):228–232.
[24] Belgardt, B.F., Okamura, T., Bruning, J.C., 2009. Hormone and glucose signalling in POMC and AgRP neurons. The Journal of Physiology 587(Pt 22):5305–5314.
[25] Bettelheim, F., Brown, W., Campbell, M., Farrall, S., 2010. Bioenergetics: how the body converts food to energy, in introduction to general, organic and biochemistry. Belmont, USA: Brooks/Cole, Cengage Learning. p. 726–46.
[26] Grundlingh, J., Dargan, P.I., El-Zanfaly, M., Wood, D.M., 2011. 2,4-Dinitrophenol (DNP): a weight loss agent with significant acute toxicity and risk of death. Journal of Medical Toxicology 7(3):205–212.
[27] Enriori, P.J., Sinnayah, P., Simonds, S.E., Garcia Rudaz, C., Cowley, M.A., 2011. Leptin action in the dorsomedial hypothalamus increases sympathetic tone to brown adipose tissue in spite of systemic leptin resistance. Journal of Neuroscience 31(34):12189–12197.
[28] Chao, P.T., Yang, L., Aja, S., Moran, T.H., Bi, S., 2011. Knockdown of NPY expression in the dorsomedial hypothalamus promotes development of brown adipocytes and prevents diet-induced obesity. Cell Metabolism 13(5):573–583.
[29] Dodd, G.T., Decherf, S., Loh, K., Simonds, S.E., Wiede, F., Balland, E., et al., 2015. Leptin and insulin act on POMC neurons to promote the browning of white fat. Cell 160(1–2):88–104.
[30] Cowley, M.A., Smart, J.L., Rubinstein, M., Cerdan, M.G., Diano, S., Horvath, T.L., et al., 2001. Leptin activates anorexigenic POMC neurons through a neural network in the arcuate nucleus. Nature 411(6836):480–484.
[31] Cowley, M.A., Smith, R.G., Diano, S., Tschop, M., Pronchuk, N., Grove, K.L., et al., 2003. The distribution and mechanism of action of ghrelin in the CNS demonstrates a novel hypothalamic circuit regulating energy homeostasis. Neuron 37(4):649–661.
[32] Rosen, E.D., Spiegelman, B.M., 2014. What we talk about when we talk about fat. Cell 156(1–2):20–44.
[33] Orellana, J.A., Saez, P.J., Cortes-Campos, C., Elizondo, R.J., Shoji, K.F., Contreras-Duarte, S., et al., 2012. Glucose increases intracellular free Ca(2+) in tanycytes via ATP released through connexin 43 hemichannels. Glia 60(1):53–68.
[34] Yang, L., Qi, Y., Yang, Y., 2015. Astrocytes control food intake by inhibiting AGRP neuron activity via adenosine A1 receptors. Cell Reports 11(5):798–807.
[35] Cortes-Campos, C., Elizondo, R., Carril, C., Martinez, F., Boric, K., Nualart, F., et al., 2013. MCT2 expression and lactate influx in anorexigenic and orexigenic neurons of the arcuate nucleus. PloS one 8(4):e62532.
[36] Cortes-Campos, C., Elizondo, R., Llanos, P., Uranga, R.M., Nualart, F., Garcia, M.A., 2011. MCT expression and lactate influx/efflux in tanycytes involved in glia-neuron metabolic interaction. PloS one 6(1):e16411.
[37] Coppola, A., Liu, Z.W., Andrews, Z.B., Paradis, E., Roy, M.C., Friedman, J.M., et al., 2007. A central thermogenic-like mechanism in feeding regulation: an interplay between arcuate nucleus T3 and UCP2. Cell Metabolism 5(1):21–33.
[38] Toda, C., Kim, J.D., Impellizzeri, D., Cuzzocrea, S., Liu, Z.W., Diano, S., 2016. UCP2 regulates mitochondrial fission and ventromedial nucleus control of glucose responsiveness. Cell 164(5):872–883.
[39] Kong, D., Vong, L., Parton, L.E., Ye, C., Tong, Q., Hu, X., et al., 2010. Glucose stimulation of hypothalamic MCH neurons involves K(ATP) channels, is modulated by UCP2, and regulates peripheral glucose homeostasis. Cell Metabolism 12(5):545–552.
[40] Hoch, F.L., Hogan, F.P., 1973. Hyperthermia, muscle rigidity, and uncoupling in skeletal muscle mitochondria in rats treated with halothane and 2,4-dinitrophenol. Anesthesiology 38(3):237–243.
[41] Geisler, J.G., Marosi, K., Halpern, J., Mattson, M.P., 2017. DNP, mitochondrial uncoupling, and neuroprotection: a little dab'll do ya. Alzheimers Dement 13(5):582–591.
[42] Korde, A.S., Pettigrew, L.C., Craddock, S.D., Maragos, W.F., 2005. The mitochondrial uncoupler 2,4-dinitrophenol attenuates tissue damage and improves mitochondrial homeostasis following transient focal cerebral ischemia. Journal of Neurochemistry 94(6):1676–1684.
[43] Wu, Y.N., Munhall, A.C., Johnson, S.W., 2011. Mitochondrial uncoupling agents antagonize rotenone actions in rat substantia nigra dopamine neurons. Brain Research 1395:86–93.
[44] Liu, D., Lu, C., Wan, R., Auyeung, W.W., Mattson, M.P., 2002. Activation of mitochondrial ATP-dependent potassium channels protects neurons against ischemia-induced death by a mechanism involving suppression of Bax

translocation and cytochrome c release. Journal of Cerebral Blood Flow Metabolism 22(4):431—443.

[45] De Felice, F.G., Ferreira, S.T., 2006. Novel neuroprotective, neuritogenic and anti-amyloidogenic properties of 2,4-dinitrophenol: the gentle face of Janus. IUBMB Life 58(4):185—191.

[46] Khan, R.S., Dine, K., Geisler, J.G., Shindler, K.S., 2017. Mitochondrial uncoupler prodrug of 2,4-dinitrophenol, MP201, prevents neuronal damage and preserves vision in experimental optic neuritis. Oxidative Medicine and Cellular Longevity 2017:10:Article ID 7180632.

[47] Pandya, J.D., Pauly, J.R., Nukala, V.N., Sebastian, A.H., Day, K.M., Korde, A.S., et al., 2007. Post-injury administration of mitochondrial uncouplers increases tissue sparing and improves behavioral outcome following traumatic brain injury in rodents. Journal of Neurotrauma 24(5):798—811.

[48] da Costa, R.F., Martinez, A.M., Ferreira, S.T., 2010. 2,4-Dinitrophenol blocks neurodegeneration and preserves sciatic nerve function after trauma. Journal of Neurotrauma 27(5):829—841.

[49] Goldgof, M., Xiao, C., Chanturiya, T., Jou, W., Gavrilova, O., Reitman, M.L., 2014. The chemical uncoupler 2,4-Dinitrophenol (DNP) protects against diet-induced obesity and improves energy homeostasis in mice in thermoneurtality. Journal of Biological Chemistry 289(28):19341—19350.

[50] Liu, D., Zhang, Y., Gharavi, R., Park, H.R., Lee, J., Siddiqui, S., et al., 2015. The mitochondrial uncoupler DNP triggers brain cell mTOR signaling network reprogramming and CREB pathway up-regulation. Journal of Neurochemistry 134(4):677—692.

